# Highly selective GaN-nanowire/TiO$_2$-nanocluster hybrid sensors for detection of benzene and related environment pollutants

**Geetha S Aluri**[1,2]**, Abhishek Motayed**[1,3,5]**, Albert V Davydov**[1]**, Vladimir P Oleshko**[1]**, Kris A Bertness**[4]**, Norman A Sanford**[4] **and Mulpuri V Rao**[2]

[1] Material Measurement Laboratory, National Institute of Standards and Technology, Gaithersburg, MD 20899, USA
[2] Department of Electrical and Computer Engineering, George Mason University, Fairfax, VA 22030, USA
[3] Institute for Research in Electronics and Applied Physics, University of Maryland, College Park, MD 20742, USA
[4] Physical Measurement Laboratory, National Institute of Standards and Technology, Boulder, CO 80305, USA

E-mail: amotayed@nist.gov

**Abstract**
Nanowire–nanocluster hybrid chemical sensors were realized by functionalizing gallium nitride (GaN) nanowires (NWs) with titanium dioxide (TiO$_2$) nanoclusters for selectively sensing benzene and other related aromatic compounds. Hybrid sensor devices were developed by fabricating two-terminal devices using individual GaN NWs followed by the deposition of TiO$_2$ nanoclusters using RF magnetron sputtering. The sensor fabrication process employed standard microfabrication techniques. X-ray diffraction and high-resolution analytical transmission electron microscopy using energy-dispersive x-ray and electron energy-loss spectroscopies confirmed the presence of the anatase phase in TiO$_2$ clusters after post-deposition anneal at 700 °C. A change of current was observed for these hybrid sensors when exposed to the vapors of aromatic compounds (benzene, toluene, ethylbenzene, xylene and chlorobenzene mixed with air) under UV excitation, while they had no response to non-aromatic organic compounds such as methanol, ethanol, isopropanol, chloroform, acetone and 1,3-hexadiene. The sensitivity range for the noted aromatic compounds except chlorobenzene were from 1% down to 50 parts per billion (ppb) at room temperature. By combining the enhanced catalytic properties of the TiO$_2$ nanoclusters with the sensitive transduction capability of the nanowires, an ultra-sensitive and selective chemical sensing architecture is demonstrated. We have proposed a mechanism that could qualitatively explain the observed sensing behavior.

(Some figures in this article are in colour only in the electronic version)

## 1. Introduction

Detection of chemical species in air such as industrial pollutants, poisonous gases, chemical fumes and volatile organic compounds (VOCs) is vital for the health and safety of communities around the world [1]. Due to their small size, ease of deployment and low-power operation, solid-state thin film sensors are often favored over analytical techniques like optical and mass spectroscopy, and gas chromatography when it comes to real-time environmental monitoring [2–4].

[5] Author to whom any correspondence should be addressed.

Selectivity, which is a sensor's ability to discriminate between the components of a gas mixture and provide a detection signal for the component of interest, is crucial for its real-life applicability. Metal-oxide-based thin film sensors, despite their commercial success and decades of research and development [5–7], still lack selectivity for different species, and often require high working temperatures [8–10]. This severely limits their usability and poses long-term reliability problems.

For a chemical sensor, the active surface area is one of the important factors determining its detection limits or sensitivity. It is well known that the electrical properties of NWs change significantly in response to their environments due to their high surface to volume ratio [11–14]. Nanowires are well suited for direct measurement of changes in their electrical properties (e.g. conductance/resistance, impedance) when exposed to various analytes. Substantial research has demonstrated the enhanced sensitivity, reactivity and catalytic efficiency of the nanoscale structures [11, 15–20]. Unfortunately, the surface/adsorbate interactions of the nanowires are limited and non-specific. Despite being electrically sensitive, nanowires still suffer from the same lack of selectivity as their bulk counterpart devices.

The idea of functionalizing or decorating the NW surface with metal or metal oxide nanoparticles or nanoclusters aims at resolving the deficiencies of such NW-based sensors. When carefully selected metal/metal oxide nanoparticles are placed on the surface of a nanowire, significant changes can result in the physical properties of the system. The nanoparticles can increase the adsorption of chemical species by introducing additional adsorption sites, thus increasing the sensitivity of such a system. Also, the metal or metal oxide nanoparticles can be selected to act as catalysts designed to lower the activation energy of a specific reaction, which produces active radicals by dissociating the adsorbed species. These radicals can then spill over to the semiconductor [21, 22] where they can be more effective in charge carrier transfer. Finally, the nanoparticles can modulate the current through the nanowire through the formation of a nanosized depletion region [23], which is in turn a function of the adsorption on the nanoparticles. In the last few years, there have been impressive demonstrations of hybrid gas sensors based on nanotubes/nanowires decorated with nanoparticles of metal and metal oxides. Leghrib *et al* reported gas sensors based on multi-wall carbon nanotubes (CNTs) decorated with tin oxide ($SnO_2$) nanoclusters for detection of NO and CO [24]. Using mixed $SnO_2/TiO_2$ included with CNTs, Duy *et al* demonstrated ethanol sensing at a working temperature of 250 °C [25]. Balázsi *et al* fabricated hybrid composites of hexagonal $WO_3$ powder with metal-decorated CNTs for sensing $NO_2$ at room temperature [26]. Kuang *et al* demonstrated an increase in the sensitivity of $SnO_2$ nanowire sensors to $H_2S$, CO and $CH_4$ by surface functionalization with ZnO or NiO nanoparticles [27]. ZnO NWs decorated with Pt nanoparticles were used by Zhang *et al*, and they showed that the response of Pt nanoparticle-decorated ZnO NWs to ethanol is three times higher than that of bare ZnO NWs [28]. Chang *et al* showed that, by adsorption of Au nanoparticles on ZnO NWs, the sensor sensitivity to CO gas could be

enhanced significantly [29]. Dobrokhotov *et al* constructed a chemical sensor from mats of GaN NWs decorated with Au nanoparticles and tested their sensitivity to $N_2$ and $CH_4$ [30]. GaN NWs coated with Pd nanoparticles were employed for the detection of $H_2$ in $N_2$ at 300 K by Lim *et al* [31].

All these results clearly demonstrate the potential of the nanowire–nanocluster-based hybrid sensors. However, there are still fundamental questions and challenges, which have not been investigated properly. Most of the reports are on mats of nanowires. Although this often increases the sensitivity, the complex nature of inter-wire conduction makes interpreting the results difficult. Also, few reports have actually shown room-temperature operation, and the selectivity is often shown for a very limited number of chemicals. The majority of highly sensitive hybrid nanowire–nanocluster devices developed so far require high operating temperatures ($\geqslant 250$ °C) and large response times (more than 5 min). Room-temperature operation of nanowire–nanocluster devices has been demonstrated by several groups but reported sensitivities were quite low with long response times. Very few research groups have actually demonstrated operation of the sensors with air as the carrier gas. However, the ability of a sensor to detect chemicals in air is what ultimately determines its usability in real life.

Our approach described in this paper utilizes n-type (Si-doped) GaN NWs functionalized with $TiO_2$ nanoclusters for selectively sensing benzene and related aromatic environmental pollutants such as toluene, ethylbenzene and xylene. This group of chemicals is commonly referred to as BTEX. GaN is a wide-bandgap semiconductor (3.4 eV), with many unique properties [32]. Its chemical inertness and capability of operating in extreme environments (high temperatures, presence of radiation, extreme pH levels) is highly desirable for sensor design. $TiO_2$ is a photocatalytic semiconductor with a bandgap energy of 3.2 eV (anatase phase). Photocatalytic oxidation of various organic contaminants over titanium dioxide ($TiO_2$) has been studied for decades [33–35]. The $TiO_2$ nanoclusters were selected to act as nanocatalysts to increase the sensitivity, lower the detection time and, most importantly, enable us to tailor the selectivity of these structures to organic analytes.

## 2. Experimental details

The NWs used in this study were *c*-axis, n-type, Si-doped GaN grown by catalyst-free molecular beam epitaxy on Si(111) substrates. Details of the NW growth can be found elsewhere [36, 37]. The process of sensor fabrication is schematically illustrated in figure 1. Post-growth device fabrication was done by dielectrophoretically aligning the nanowires on 9 mm × 9 mm sapphire substrates [38]. These device substrates had 12 nm thick Ti alignment electrodes of semicircular geometry with gaps between them ranging from 4 to 8 $\mu$m. After the alignment of the nanowires the samples were dried at 75 °C for 10 min on a hot plate for evaporation of the residual solvent. This was followed by a plasma-enhanced chemical vapor deposition (PECVD) of 50 nm of $SiO_2$ at a deposition temperature of 300 °C. This passivation layer was

Legend:
- Sapphire substrate
- Alignment electrode: Ti (12 nm)
- GaN nanowire
- 50 nm PECVD SiO$_2$
- TiO$_2$ nanocluster
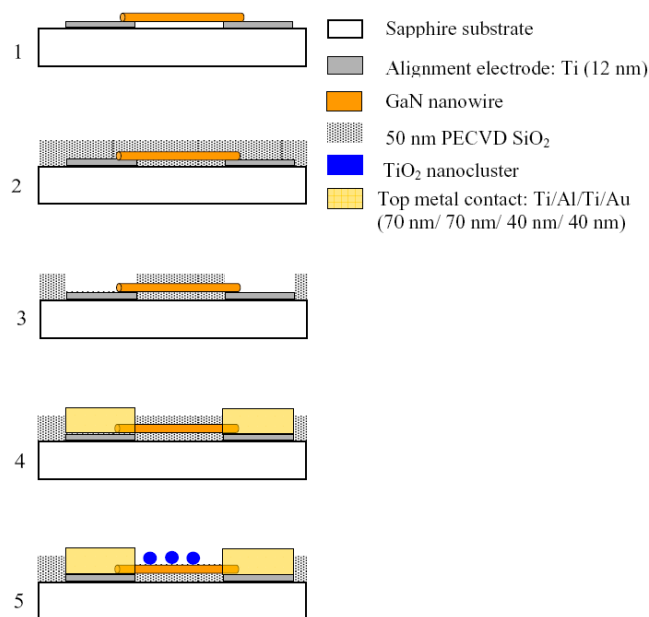- Top metal contact: Ti/Al/Ti/Au (70 nm/ 70 nm/ 40 nm/ 40 nm)

**Figure 1.** Schematic representation of the hybrid sensor fabrication process (not drawn to scale).

deposited to ensure a higher yield for the fabrication process. After the oxide deposition, photolithography was performed to define openings for the top contact.

The oxide in the openings was etched using reactive ion etching (RIE) with CF$_4$/CHF$_3$/O$_2$ (50 sccm/25 sccm/5 sccm) gas chemistry. The top contact metallization was deposited in an electron beam evaporator with base pressure of $10^{-5}$ Pa. The deposition sequence was Ti (70 nm)/Al (70 nm)/Ti (40 nm)/Au (40 nm). The oxide layer over the nanowires between the end contacts was then etched in buffered HF etching solution for 15 s. A negative resist is used to protect the end metal contacts from the etching solution. The TiO$_2$ nanoclusters were deposited on the exposed GaN NWs using RF magnetron sputtering. The deposition was done at 325 °C with 50 sccm of Ar flow and 300 W RF power. The deposition rate was about 0.2 Å s$^{-1}$. Thermal annealing of the complete sensor devices (GaN NW with TiO$_2$ nanoclusters) was done at 650 °C to 700 °C for 30 s in a rapid thermal processing system with 6 slpm (standard liter per min) flow of ultrahigh purity Ar. A relatively slow ramp rate of 100 °C min$^{-1}$ was chosen to reduce the stress in the metal–nanowire contact area during heating. The anneal step was optimized to facilitate ohmic contact formation to the GaN NWs and also to induce crystallization of the TiO$_2$ clusters. Additional lithography was performed to form thick metal bond pads with Ti (40 nm) and Au (160 nm).

The crystallinity and phase analysis of the sputtered TiO$_2$ films were assessed by x-ray diffraction (XRD). The XRD scans were collected on a Bruker-AXS D8 scanning x-ray microdiffractometer equipped with a general area detector diffraction system (GADDS) using Cu K$\alpha$ radiation[6]. The

two-dimensional 2Θ-$\chi$ patterns were collected in the 2Θ = 23°–51° range followed by integration into conventional Ω-2Θ scans. The microstructure and morphology of the sputtered TiO$_2$ films used for the fabrication of sensors were characterized by high-resolution analytical transmission and scanning transmission electron microscopy (HRTEM/STEM) and cold field emission scanning electron microscopy (FESEM). GaN nanowires with sputtered TiO$_2$ were deposited onto a lacey carbon film supported by Cu-mesh grids and analyzed in a 300 kV TEM/STEM microscope. The instrument was equipped with an x-ray energy-dispersive spectrometer (XEDS) and an electron energy-loss spectrometer (EELS) as well as bright-field (BF) and annular dark-field (ADF) STEM detectors to perform spot and line profile analyses.

The device substrates, i.e. the sensor chips, were wire-bonded on a 24-pin ceramic package for the gas sensing measurements. The device characterization and the time-dependent sensing measurements were done using an Agilent B1500A semiconductor parameter analyzer. Each sensor chip was placed in a custom-designed stainless steel test chamber of volume 0.73 cm$^3$ with separate gas inlet and outlet. The test chamber had a quartz window on top for UV excitation provided by a 25 W deuterium bulb (DH-2000-BAL, Ocean Optics) connected to a 600 $\mu$m diameter optical fiber cable with a collimating lens at the end for uniform illumination over the sample surface. The operating wavelength range of the bulb was 215–400 nm. The intensity at 365 nm measured using an optical power meter was 375 nW cm$^{-2}$. For all the sensing experiments regular breathing air (<9 ppm of water) was used as the carrier gas. A wide range of concentrations from 1% to as low as 50 parts per billion (ppb) of various organic compounds were achieved with a specific arrangement of bubbler and mass flow controllers (MFCs). During the sensor measurements, the net flow (air + VOC mix) into the test chamber was set to a constant value of 20 sccm. After the sensor devices were exposed to the organic compounds, they were allowed to regain their baseline current with the air–chemical mixture turned off, without purging or evacuating the test chamber.

## 3. Results

Figure 2 shows GaN nanowires with three different nominal thicknesses of TiO$_2$ coatings sputtered on them. Rather sparse, well-defined clusters can be seen for both the 5 and 8 nm area-averaged sputtered coatings of TiO$_2$. The average size of these large clusters was 15 nm. For the 8 nm sputtered coating the coverage of the TiO$_2$ clusters is much denser. However, TEM studies revealed the presence of clusters with much smaller diameter ($\sim$ less than 4 nm) on the nanowire surface. For all the sensors we have used only 8 nm deposits of TiO$_2$.

Since we were unable to detect the XRD signal from the TiO$_2$-decorated GaN NWs due to the minuscule size and total volume of TiO$_2$ nanoclusters, we prepared a 150 nm thick TiO$_2$ film by sputtering it onto an SiO$_2$-coated Si substrate at 300 °C followed by a anneal at 650 °C for 45 s in argon. The
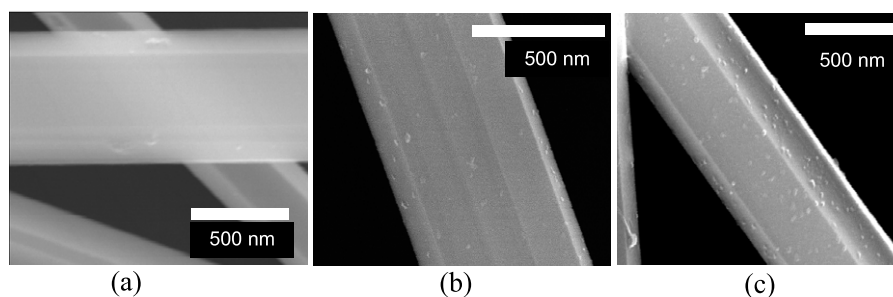
**Figure 2.** FESEM images of three different sputtered thickness of TiO$_2$ coatings: (a) 2 nm, (b) 5 nm and (c) 8 nm of TiO$_2$ sputtered on GaN nanowires.
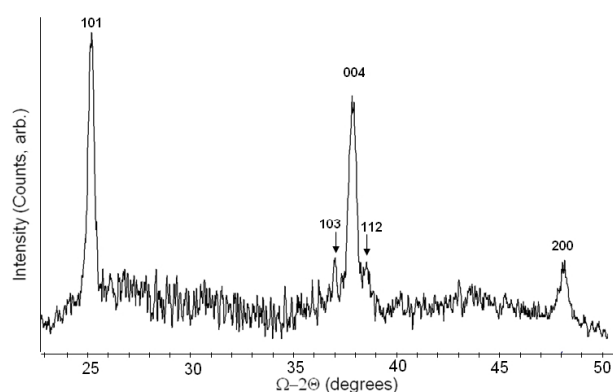


**Figure 3.** XRD $\Omega - 2\Theta$ scan of 150 nm thick TiO$_2$ film deposited on SiO$_2$/Si substrate at 300 °C and annealed at 650 °C for 45 s in RTA. All indices correspond to the anatase phase (PDF#84-1285).

assumption was made that this processing conditions produced an identical morphology as in the TiO$_2$-decorated NW case. We identified from the XRD in figure 3 that TiO$_2$ is in the single-phase anatase form. As-deposited TiO$_2$ films were found to be amorphous (XRD not shown). The XRD results agree with the TEM analysis on TiO$_2$-decorated GaN NWs,

which revealed that, upon annealing at 700 °C for 30 s, the TiO$_2$ islands became partially crystalline (see figure 4). The three most common phases of TiO$_2$ are anatase, rutile and brookite. Thermodynamic calculations predict that rutile is the most stable TiO$_2$ phase in the bulk state at all temperatures and atmospheric pressure [39, 40]. However, comparative experiments with particle size showed that the phase stability might reverse with decreasing particle size, possibly due to the influence of surface free energy and surface stress [41]. Anatase is the most stable phase when the particle size is less than 11 nm, whereas rutile is most stable at sizes greater than 35 nm [42]. Although both rutile and anatase TiO$_2$ are commonly used as photocatalysts, the anatase form shows greater photocatalytic activity for most reactions [43, 44]. This is one of the reasons why we have sputtered nominally 8 nm of TiO$_2$ for the sensor fabrication.

Although we have sputtered 8 nm of TiO$_2$ for fabricating our hybrid sensors, for the TEM studies we used 20 nm of TiO$_2$ coating. This was done because the thick GaN nanowires prevented us from acquiring any TEM diffraction from thinner TiO$_2$ coatings. The TEM results presented here for 20 nm thick TiO$_2$ are assumed to be representative of the clusters formed for 8 nm deposited TiO$_2$ in actual sensors. Typical morphologies of a 20 nm thick TiO$_2$ film sputtered
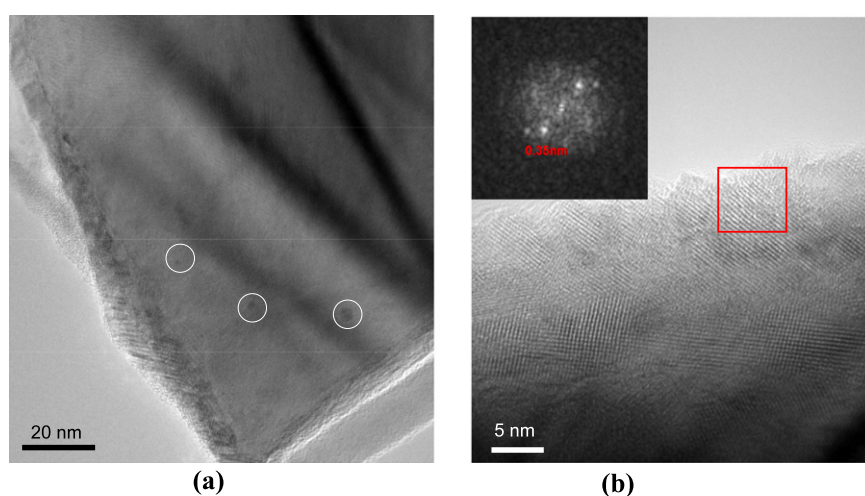


**Figure 4.** Typical morphologies of a 20 nm thick TiO$_2$ film sputtered on n-GaN nanowires and annealed at 700 °C for 30 s. (a) TEM image showing non-uniformly distributed 2–10 nm diameter individual TiO$_2$ particles, some of them marked by white circles. (b) HRTEM image of an edge of the GaN nanowire with the sputtered TiO$_2$ film, FFT pattern from the red square area in the upper inset indicates 0.35 nm lattice fringes, which are consistent with a (101) reflecting plane of anatase.
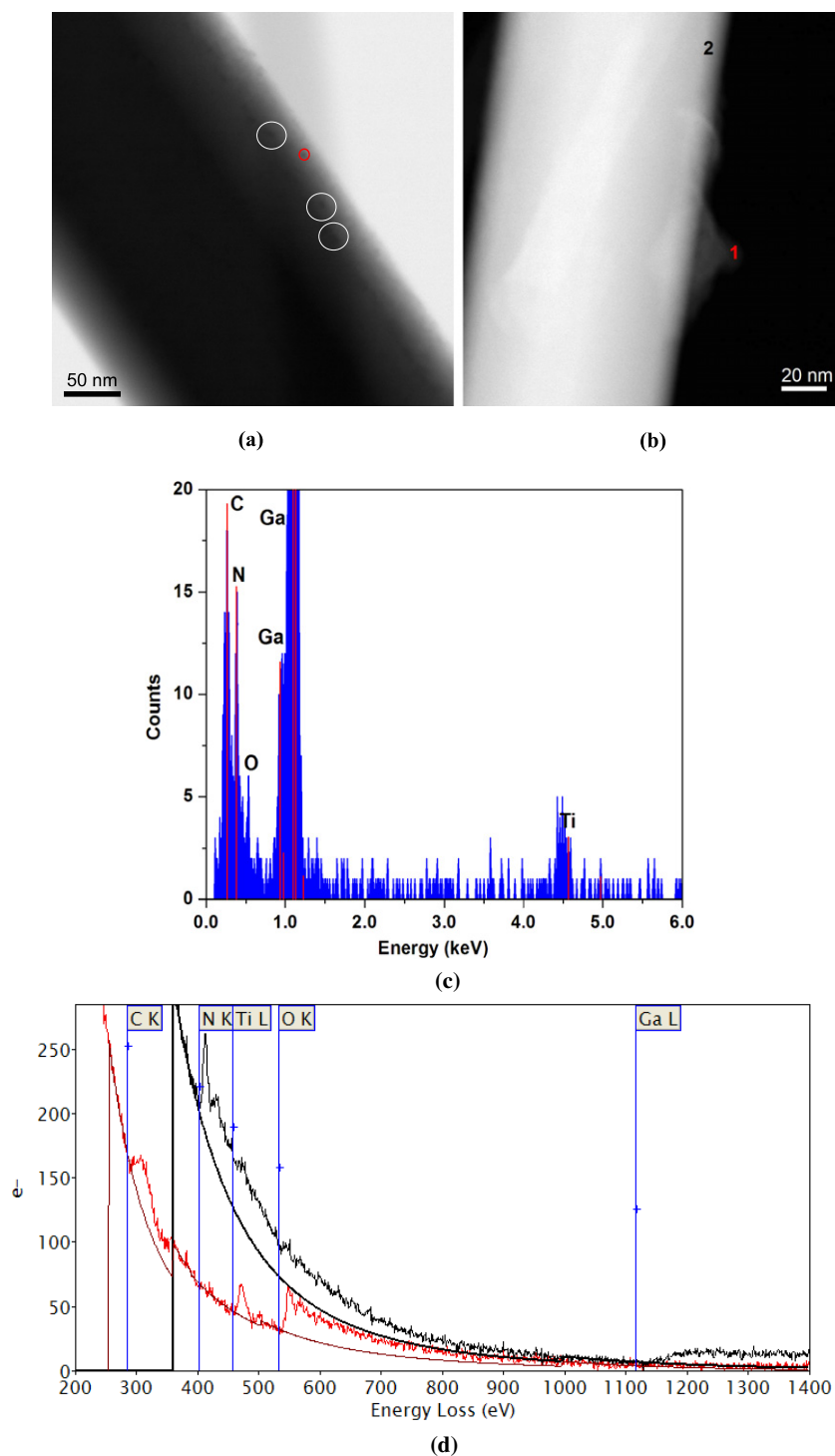
**Figure 5.** (a) BF-STEM image with 5–10 nm TiO$_2$ nanoparticles barely visible near an edge of a GaN nanowire, some of them marked by white circles. (b) ADF-STEM image of a TiO$_2$-containing aggregate on the edge of a GaN nanowire. (c) X-ray spectrum of an individual 5 nm TiO$_2$ particle shown by the red circle in the image in (a). (d) EEL spectra recorded at positions 1 (tip of the aggregate) and 2 (edge of the GaN nanowire) as shown in the image in (b), respectively.

on n-GaN nanowires and annealed at 700 °C for 30 s are illustrated by TEM data in figure 4. The TEM image in figure 4(a) shows 2–10 nm diameter individual TiO$_2$ particles non-uniformly distributed on the surface of a GaN nanowire. Some of the particles are marked by white circles. We observed crystallinity of some nanoparticles as shown in the HRTEM image in figure 4(b) of nanocrystallites on the edge of a GaN

nanowire with the sputtered TiO$_2$. The FFT pattern from the red square area in the upper inset shows 0.35 nm lattice fringes, which are consistent with a (101) reflecting plane of anatase but not available in hexagonal wurtzite-type GaN crystals.

The figure 5(a) BF-STEM image shows 5–10 nm TiO$_2$ nanoparticles barely visible against the GaN nanowire. An ADF-STEM image of a TiO$_2$ island on a GaN nanowire is
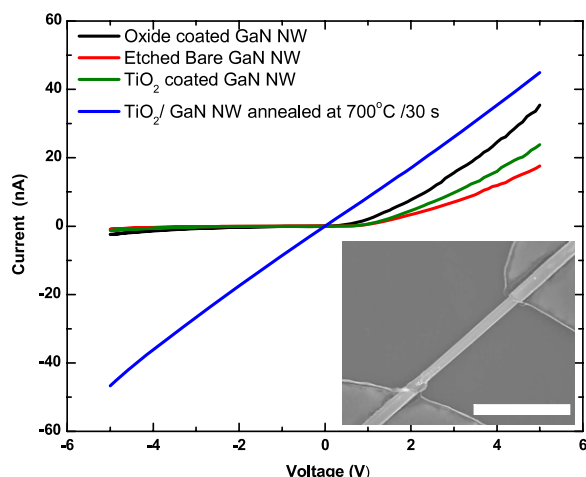
**Figure 6.** *I–V* characteristics of a GaN NW two-terminal device in the dark at different stages of processing. The inset shows the nanowire device with length 5.35 $\mu$m and diameter 380 nm. The scale bar is 4 $\mu$m. The thickness of sputtered TiO$_2$ film was 8 nm.

shown in figure 5(b). The presence of TiO$_2$ was confirmed by analysis of selected areas as well as of individual particles using XEDS and EELS and nanoprobe capabilities. The x-ray spectrum in figure 5(c) of an individual 5 nm TiO$_2$ particle marked by the red circle in figure 5(a) exhibits the Ti K$\alpha$ peak at 4.51 keV and the weak O K$\alpha$ peak at 0.523 keV. The N K$\alpha$ peak at 0.39 keV and gallium lines (the Ga L series at 1.0–1.2 keV) and the C K$\alpha$ peak at 0.28 keV are also identified. The EEL spectrum acquired at position 1 marked in figure 5(b) (the tip of a TiO$_2$-containing aggregate) exhibits the Ti L edge at 456 eV and the O K edge at 532 eV and also the C K edge at 284 eV. A reference spectrum recorded at position 2 (an edge of the GaN nanowire in figure 5(b)) still reveals traces of titanium and oxygen with the NK edge at 401 eV and the Ga L edge at 1115 eV, respectively.

Figure 6 shows the *I–V* characteristics of a GaN NW two-terminal device at different stages of processing. The *I–V* curves of the as-deposited devices were nonlinear and asymmetric. The current decreased when the SiO$_2$ layer over

the NW was etched. However, the current increased with the deposition of TiO$_2$ nanoclusters. Oxygen adsorption on the bare GaN nanowire surface can introduce surface states [45], resulting in the decrease of the nanowire conductivity. The devices annealed at 700 °C for 30 s showed significant changes in their *I–V* characteristics, with a majority of the devices exhibiting linear *I–V* curves. This is consistent with the fact that low resistance ohmic contacts to the nitrides require annealing at 700 to 800 °C [46].

Figure 7 shows the photoconductance of a bare GaN NW device and the TiO$_2$-coated GaN NW device. The NW devices with TiO$_2$ nanoclusters showed almost two orders of magnitude increase in the current when exposed to UV light as compared to the similar-diameter bare NW devices. Increase of photoconductance due to surface functionalization has been observed in ZnO nanobelts coated with different polymers [47]. This enhancement of photoconductance is often attributed to the separation of photogenerated charge carriers by a surface depletion field, thereby increasing the lifetime of the photogenerated carriers. After the light is turned off, the photocurrent decays rapidly but not to the dark current value, which is probably due to the persistent photoconductivity of the NWs [48].

The current through the bare GaN NW devices did not change when exposed to different VOCs mixed in air, even for concentrations as high as a few percent. On the other hand, the TiO$_2$-coated hybrid devices responded even to the pulses of 20 sccm airflow. This is not surprising considering the fact that the conduction in most metal oxides is affected by the presence of oxygen. The response of the TiO$_2$-nanocluster–GaN-nanowire hybrid sensor to 1000 ppm of toluene in air is illustrated in figure 8. Exposure to the VOCs in the dark has no effect on the hybrid device. However, in the presence of UV excitation, when 1000 ppm of toluene (mixed in air) was introduced into the gas chamber, the sensor photocurrent decreased dramatically to approximately 2/3 of its base value. After 100 s of gas exposure, the gas flow is turned off and the sensor is allowed to recover at room temperature without any additional purging. The repeatability of the sensing action of these hybrid sensors is evident from figure 8.
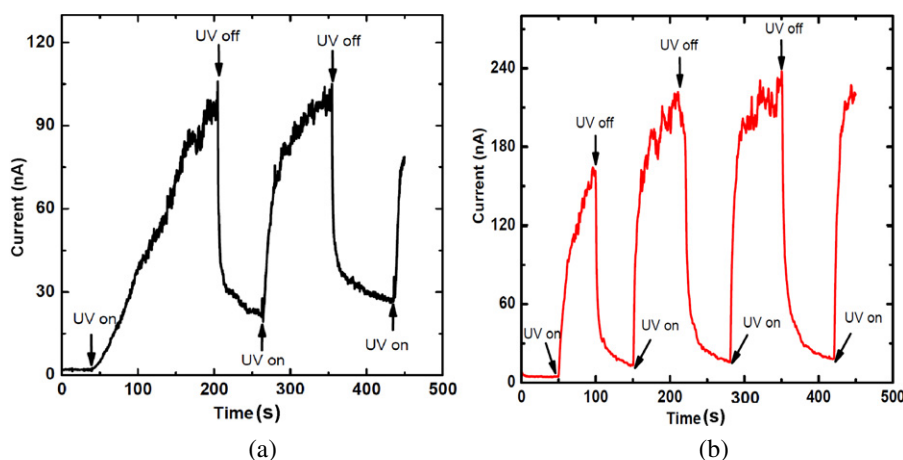


(a)



(b)

**Figure 7.** (a) Dynamic photocurrent of a bare GaN NW and (b) of a TiO$_2$-coated (8 nm deposit) GaN NW. The diameters of both nanowires were ~200 nm. The applied bias is 5 V in both cases.
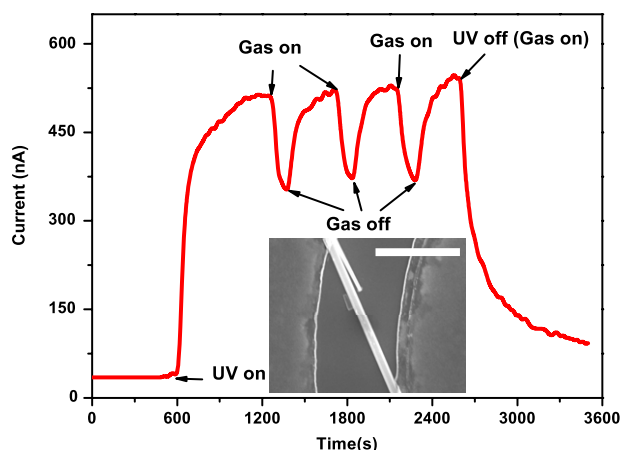
**Figure 8.** Dynamic response of a single GaN–TiO$_2$ hybrid device to 1000 ppm of toluene. For each cycle the gas exposure time was 100 s. Inset shows the nanowire device with 8.0 $\mu$m length and diameter 500 nm. The scale bar is 5 $\mu$m.

Interestingly, these hybrid sensors did not respond when exposed to methanol, ethanol, isopropanol, chloroform, acetone and 1,3-hexadiene, even for concentrations as high as several percent. Also, the photocurrent for these sensors increased with respect to air when exposed to toluene vapor, whereas for every other aromatic compound the photocurrent decreased relative to air, as seen in figure 9(a). We tested more than 20 sensor devices and they all exhibited the same trend. We used toluene from different sources and the sensor behavior was the same. Figure 9(b) shows the response of a different device for 200 ppb concentrations of the same chemicals. It is clear that, even for toluene concentrations as low as 200 ppb the relative change in photocurrent is the reverse of that observed with other chemicals. If the photocurrent in the presence of air for these sensors is used as their baseline calibration, then we can distinctly identify toluene from other

---

[7] We were not able to measure the response of the device to chlorobenzene below 10 ppm due to limitation of our gas delivery set-up.

aromatic compounds present in air using our hybrid devices. The response time is defined as the time taken by the sensor current to reach 90% of the response ($I_f - I_0$) when exposed to the analyte. $I_f$ is the steady sensor current level in the presence of the analyte and $I_0$ is the current level without the analyte, which in our case is in the presence of air. The recovery time is the time required for the sensor current to recover to 30% of the response ($I_f - I_0$) after the gas flow is turned off [49]. For our sensors the response and recovery times for ppm levels of BTEX concentrations are ≈60 s and ≈75 s, respectively. The response and recovery times for ppb levels of concentrations are ≈180 s and ≈150 s, respectively. Most of the nanoparticle-decorated nanowire/nanotube sensors reported in the literature working at room temperatures had response times in minutes [24, 26, 27, 31]. Fast response and recovery times indicate fast adsorption and desorption, which could be attributed to the enhanced reactivity of the nanoscale TiO$_2$ clusters.

The responses of two hybrid devices to different concentrations of toluene in air are shown in figure 10. Figure 10(a) shows the change of photocurrent of a 234 nm diameter device when exposed to toluene concentrations from 10 000 ppm down to 100 ppm. Figure 10(b) shows the photocurrent of a sensor device with 170 nm diameter wire for toluene concentrations from 1 ppm to 50 ppb.

We have defined the sensitivity as ($R_{\mathrm{gas}} - R_{\mathrm{air}})/R_{\mathrm{air}}$, where $R_{\mathrm{gas}}$ and $R_{\mathrm{air}}$ are the resistances of the sensor in the presence of the chemical–air mixture and in the presence of air, respectively. The sensitivity plots of a hybrid device for different VOCs tested are shown in figure 11. The sensitivity plot emphasizes the ability of these hybrid sensors to reliably detect BTEX (benzene, toluene, ethylbenzene and xylene)—the common indoor and outdoor pollutants with wide detection range (50 ppb to 1%).

## 4. Discussions

In the previous section, we have demonstrated GaN–TiO$_2$ (nanowire–nanocluster) hybrid sensors and measured their
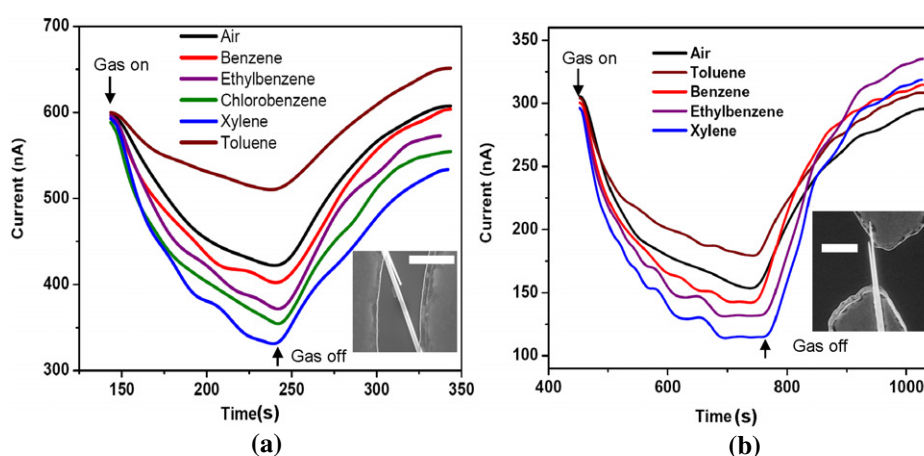


**Figure 9.** (a) Response of a single nanowire–nanocluster hybrid sensor (inset shows nanowire with diameter 500 nm) to 1000 ppm benzene, toluene, ethylbenzene, chlorobenzene and xylene in presence of UV excitation. (b) Response of a different sensor (inset shows nanowire with diameter 300 nm) to 200 ppb toluene, benzene, ethylbenzene and xylene[7] with UV excitation. The total flow into the chamber was kept constant at 20 sccm. The response with air is also shown. The scale bars are 5 $\mu$m.
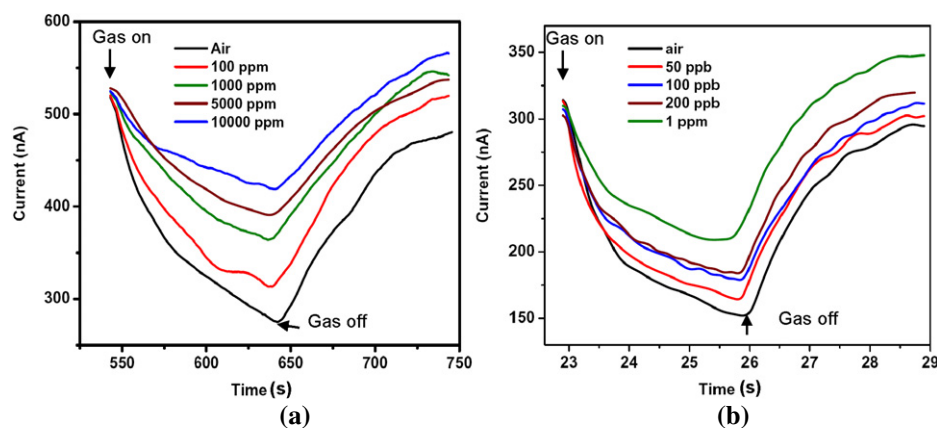
**Figure 10.** Hybrid sensor's photoresponse characteristics: (a) device shown in figure 9(a) for 100–10 000 ppm concentration range of toluene and (b) device shown in figure 9(b) for 50 ppb to 1 ppm concentration range of toluene.
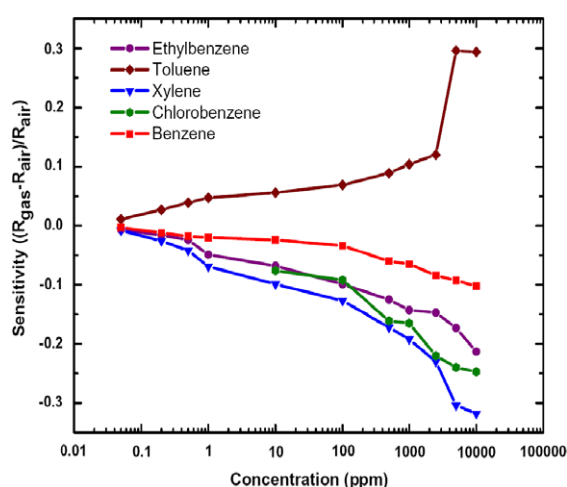


**Figure 11.** Sensitivity plots of a GaN–TiO₂ nanowire–nanocluster hybrid device (diameter 300 nm) for benzene, toluene, ethylbenzene, chlorobenzene and xylene. The plot identifies the sensor's ability to measure a wide range of concentrations of the indicated chemicals.

response to specific volatile organic compounds mixed with air at ambient temperature and humidity. In the presence of UV light these hybrid sensor devices exhibited a change in the photocurrent when exposed to benzene, toluene, ethylbenzene, xylene and chlorobenzene mixed in air. On the other hand, gases like methanol, ethanol, isopropanol, chloroform, acetone and 1,3-hexadiene did not induce any change in the electrical characteristics of the devices, which clearly demonstrated the selective response of these sensors to the aromatic compounds. We were able to detect benzene, toluene, ethylbenzene and xylene at concentration levels as low as 50 ppb in air. These sensor devices were highly stable and able to sense aromatic compounds in air reliable for a wide range of concentration (50 ppb to 1%). Based on these findings and results of structural analysis, we can propose the following mechanism (see figure 12) that can qualitatively explain the hybrid sensor's response to different analytes. Although there are still debates over the exact mechanisms responsible for the photocatalytic processes on the TiO₂ surface, it is now well established that

the oxygen vacancy defects ($Ti^{3+}$ sites) on the surface of $TiO_2$ are the 'active sites' responsible for adsorption of species like oxygen, water and organic molecules [50]. It is interesting to note that a relatively defect-free $TiO_2$ surface, generated by annealing in high oxygen flux, is chemically inactive [51].

It has been revealed in both experimental studies and simulations that molecular oxygen is chemisorbed on the surface vacancies ($Ti^{3+}$ sites) acquiring a negative charge as shown in figure 12(a) [52, 53]. This is believed to be due to the presence of the localized electron density at or near exposed $Ti^{3+}$ atoms on the $TiO_2$ surface [54]. Water could also be present on the $TiO_2$ cluster surface via molecular or dissociative adsorption (producing $OH^-$ species) on the defect sites [55, 56]. Although most of the theoretical and experimental studies on oxygen and water adsorption are done for the (110) surface of the rutile phase, there are some studies that suggest that similar adsorption behavior is also expected for the anatase surface [57]. The GaN NW has a surface depletion region as shown in figure 12(a) which determines its dark conductivity [48]. In the presence of UV excitation with an energy above the bandgap energy of anatase $TiO_2$ (3.2 eV) and GaN (3.4 eV), electron–hole pairs are generated both in the GaN NW and in the $TiO_2$ cluster as shown in figure 12(b). Photogenerated holes in the nanowire tend to diffuse toward the surface due to the surface band bending. As mentioned before, this effect of separation of photogenerated charge carriers results in a longer lifetime of photogenerated electrons, which in turn enhances the photoresponse of the nanowire devices in general. On the $TiO_2$ cluster surface, however, the photogenerated charge carriers lead to a different phenomenon. In n-type semiconductor oxides such as $TiO_2$ the surface adsorption produces upward band bending, which drives the photogenerated holes towards the surface. The chemisorbed oxygen molecule ($O_2^-$) and hydroxide ions ($OH^-$) can readily capture a hole and desorb as shown in figure 12(b) [58, 59]. The decrease of photocurrent through these hybrid sensors when exposed to 20 sscm of air could be due to the increase in oxygen concentration at the surface of $TiO_2$ clusters, leading to an increase in trapping of photogenerated holes at the surface. This process results in an increased lifetime of photogenerated
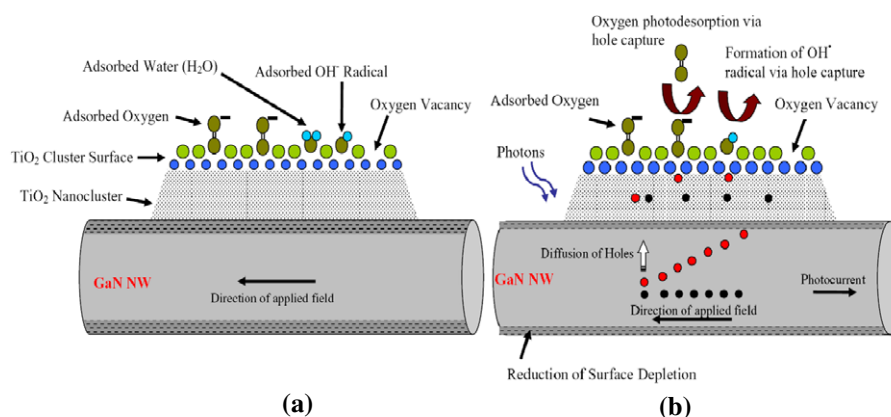
**Figure 12.** Schematic representation of the GaN (nanowire)–TiO$_2$ (nanocluster) hybrid sensor (not to scale) (a) in the dark showing surface depletion of the GaN nanowire and (b) under UV excitation, where photodesorption of O$_2$ due to hole capture is shown.
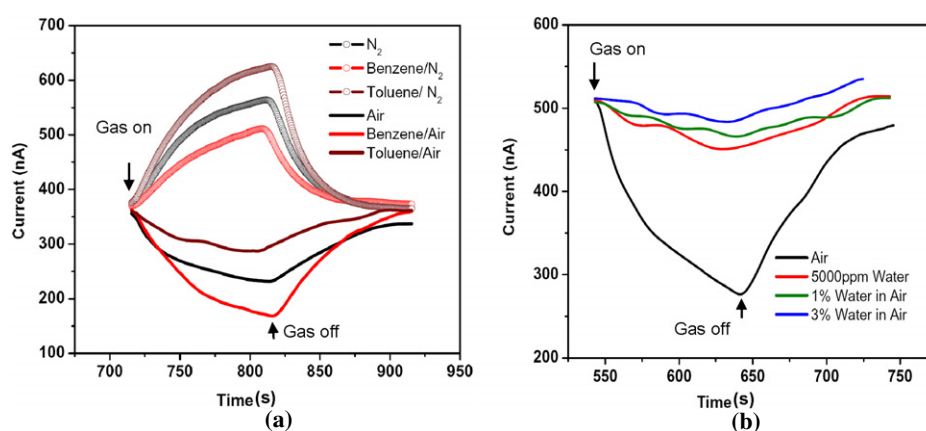


**Figure 13.** (a) Photoresponse of a hybrid device (diameter 300 nm) to 1000 ppm of benzene and toluene mixed in air and nitrogen. (b) Response of a hybrid device (diameter 500 nm) to different concentrations of water in air.

electrons. As these nanowires are n-type, excess negative charge on the surface of the wire (on the TiO$_2$ clusters) will reduce the nanowire current, which can be thought of as a local-gating effect due to net negative charge accumulation in the TiO$_2$ clusters. The adsorbed hydroxyl ions could also trap a hole forming OH$^.$ species. There could be other effects such as diffusion of carriers between the clusters and the nanowire, which could have a major role in the sensing properties of these hybrids.

Our hypothesis could also explain the sensor response when exposed to N$_2$ flow, as shown in figure 13(a). In the presence of 20 sccm of N$_2$ flow, the photocurrent in these sensors increased significantly in comparison with 20 sccm of air flow. In the N$_2$ environment, oxygen is desorbed from the surface vacancy sites by capturing photogenerated holes, but does not get readsorbed, resulting in a significant reduction of hole capture. So the photogenerated electron–hole pairs recombine effectively in the cluster. Thus the photocurrent through the nanowire/nanocluster hybrid is increased because the local-gating effect due to the TiO$_2$ clusters is absent in the N$_2$ environment.

In the presence of water in air the photocurrent through these sensors recovers towards the level without air flow as

seen in figure 13(b), indicating possible reduction of the hole trapping due to adsorption of water on the TiO$_2$ surface. Water could be adsorbed as a molecule on the defect sites replacing O$_2$ [60]. With increasing water concentration more defects are filled with water. As mentioned before, if the adsorbed water dissociates producing OH$^-$ species, then it is possible that it can also act as hole traps and decrease the photocurrent the same way the photodesorption of oxygen does. Perhaps there is a competition between the molecular water adsorption (reducing hole capture) and dissociative water adsorption (increasing hole capture), with the dominant process ultimately determining the photocurrent level in the nanowires in the presence of water. The presence of aromatic compounds such as benzene, ethylbenzene, chlorobenzene and xylene in air reduced the photocurrent as seen in figure 13(a). Organic molecules are known hole trapping adsorbates [61], although details of the trapping mechanism remain elusive. Most aromatic compounds show high affinity for electrophilic aromatic substitution. There is a much debate about the exact mechanism of photo-oxidation of adsorbed organic compounds on TiO$_2$. However, there exists a significant body of literature that indicates that oxidation may occur by either indirect oxidation via the surface-bound hydroxyl radical (i.e. a trapped

**Table 1.** Physical properties of various compounds tested.

| Organic compound | Sensitivity | Ionization potential (eV) |
|---|---|---|
| Chloroform | No | 11.37 |
| Ethanol | No | 10.62 |
| Isopropanol | No | 10.16 |
| Cyclohexane | Yes | 9.98 |
| Acetone | No | 9.69 |
| Benzene | Yes (Min) | 9.25 |
| Chlorobenzene | Yes | 9.07 |
| Toluene | Yes | 8.82 |
| Ethylbenzene | Yes | 8.77 |
| Xylene | Yes (Max) | 8.52 |
| 1,3-hexadiene | No | 8.50 |

hole at the $TiO_2$ surface) or directly via the valence band hole before it is trapped either within the particle or at the particle surface [62, 63]. We can speculate that in the presence of air (with residual water) hydroxyl-mediated hole transfer to adsorbates such as benzene or xylene is dominant, whereas in the $N_2$ environment direct transfer of valence band holes to aromatic adsorbates could be possible. Irrespective of the hole transfer mechanism, the presence of additional hole traps will reduce the sensor photocurrent as observed in the presence of benzene mixed with $N_2$ and air (see figure 13(a)). Our model can at least qualitatively explain the observed trends for the four compounds tested, namely benzene, ethylbenzene, chlorobenzene and xylene. Toluene, however exhibits a different trend, which cannot be explained by the hole trapping mechanism. There could be other second-order effects that are difficult to speculate about without fundamental surface studies. We plan to use a scanning tunneling microscope to identify the adsorbed species on such nanoclusters and to shed some light on the charge transfer mechanisms in these sensors.

Our interpretation is further validated if we compare the ionization energies of various compounds tested with the responses they generated when these sensors are exposed to them (see table 1). The effectiveness of the process of hole transfer to the adsorbed organic molecules should be related to the compound's ability to donate an electron (i.e. the lower the ionization energy of a compound, the easier it is for it to donate an electron or capture a hole). The observed sensitivity trend for benzene (lowest sensitivity), ethylbenzene and xylene (highest sensitivity) correlates with their ionization energies as shown in table 1, with benzene being the highest and xylene the lowest among the three.

It is clear from table 1 that this trend holds true only for aromatics as 1,3-hexadiene did not produce any response in our sensors. Although most functional groups with either a non-bonded lone pair or p-conjugation show oxidative reactivity toward $TiO_2$ [64], aromatic compounds are more easily photocatalyzed than aliphatic ones under the same conditions [65].

## 5. Conclusions

We demonstrated highly selective and sensitive sensors using GaN nanowires decorated with $TiO_2$ nanoclusters. The significant features of our sensors are: (1) UV-induced room-temperature sensing as opposed to thermally induced sensing, which promises low-power operation, longer lifetime and fast on/off capability, (2) selective sensing of aromatic compounds with additional selectivity for methyl group substitution, i.e. these sensors can distinguish toluene from other aromatic compounds, (3) wide sensing range (50 ppb–1%), (4) fast response and recovery, and (5) reliable and repeatable operation. We speculate that photoinduced oxygen desorption and subsequent capture of holes by organic adsorbate molecules on the surface of $TiO_2$ clusters produces a local gating effect, which is responsible for the sensing action of our hybrids. This study highlights the potentials of nanowire–nanocluster hybrids for developing a new generation of highly selective and ultra-sensitive sensors for chemical and biological sensing. The detailed sensing mechanism of these hybrid sensors needs to be studied further using advanced surface-sensitive imaging and spectroscopy techniques.

## References

[1] Watson J and Ihokura K (ed) 1999 Special issue on gas-sensing materials *Mater. Res. Soc. Bull.* **24** 14
[2] Wilson D M, Hoyt S, Janata J, Booksh K and Obando L 2001 *IEEE Sensor J.* **1** 256
[3] Shimizu Y and Egashira M 1999 Basic aspects and challenges of semiconductor gas sensors *Mater. Res. Soc. Bull.* **24** 18
[4] Sze S M 1994 *Semiconductor Sensors* 1st edn (New York: Willey)
[5] Brattain J B W H 1952 *Bell. Syst. Tech. J.* **32** 1
[6] Janata J 1992 *Anal. Chem.* **64** 196
[7] Azad A M, Mhaisalkar S G, Birkefeld L D, Akbar S A and Goto K S 1992 *J. Electrochem. Soc.* **139** 2913
[8] Meixner H and Lampe U 1996 *Sensors Actuators* B **33** 198
[9] Nicoletti S, Zampolli S, Elmi I, Dori L and Severi M 2003 *IEEE Sensors J.* **3** 454
[10] Demarne V and Sanjines R 1992 *Gas Sensors-Principles, Operation and Developments* ed G Sberveglieri (The Netherlands: Kluwer Academic)
[11] Cui Y, Wei Q, Park H and Lieber C M 2001 *Science* **293** 1289
[12] Zhang D, Liu Z, Li C, Tang T, Liu X, Han S, Lei B and Zhou C 2004 *Nano Lett.* **4** 1919
[13] Kong J, Franklin N R, Zhou C, Chapline M G, Peng S, Cho K and Dai H 2000 *Science* **287** 622
[14] Comini E, Fagila G, Sberveglieri G, Pan Z and Wang Z L 2002 *Appl. Phys. Lett.* **81** 1869
[15] Li C, Zhang D, Liu X, Han S, Tang T, Han J and Zhou C 2003 *Appl. Phys. Lett.* **8** 1613
[16] Wan Q, Li Q H, Chen Y J, Wang T H, He X L, Li J P and Lin C L 2004 *Appl. Phys. Lett.* **84** 3654
[17] Wang C, Chu X and Wu M 2005 *Sensors Actuators* B **113** 320

[18] Wang H T, Kang B S, Ren F, Tien L C, Sadik P W, Norton D P and Pearton S J 2005 *Appl. Phys. Lett.* **86** 243503

[19] Raible I, Burghard M, Schlecht U, Yasuda A and Vossmeyer T 2005 *Sensors Actuators* B **106** 730

[20] McAlpine M C, Ahmad H, Wang D and Heath J R 2007 *Nat. Mater.* **6** 379

[21] Sermon P A and Bond G C 1973 *Catal. Rev.* **8** 211

[22] Conner W C Jr, Pajnok G M and Teichner S J 1986 *Adv. Catal.* **34** 1

[23] Morrison S R 1987 *Sensors Actuators* **12** 425

[24] Leghrib R, Pavelko R, Felten A, Vasiliev A, Cané A, Gràcia I, Pireaux J J- and Llobet E 2010 *Sensors Actuators* B **145** 411

[25] Duy N V, Hieu N V, Huy P T, Chien N D, Thamilselvan M and Yi J 2008 *Physica* E **41** 258

[26] Balázsi C, Sedlácková K, Llobet E and Ionescu R 2008 *Sensors Actuators* B **133** 151

[27] Kuang Q, Lao C-S, Li Z, Liu Y-Z, Xie Z-X, Zheng L-S and Wang Z L 2008 *J. Phys. Chem.* C **112** 11539

[28] Zhang Y, Xu J, Xu P, Zhu Y, Chen X and Yu W 2010 *Nanotechnology* **21** 285501

[29] Chang S-J, Hsueh T-J, Chen I-C and Huang B-R 2008 *Nanotechnology* **19** 175502

[30] Dobrokhotov V *et al* 2006 *J. Appl. Phys.* **99** 104302

[31] Lim W, Wright J S, Gila B P, Johnson J L, Ural A, Anderson T, Ren F and Pearton S J 2008 *Appl. Phys. Lett.* **93** 072109

[32] Morkoç H 1999 *Nitride Semiconductors and Devices* (New York: Springer)

[33] Mills A and Hunte S L 1997 *J. Photochem. Photobiol.* A **108** 1

[34] Luo Y and Ollis D F 1996 *J. Catal.* **163** 1

[35] Butler E C and Davis A P 1993 *J. Photochem. Photobiol.* A **70** 273

[36] Bertness K A, Roshko A, Mansfield L M, Harvey T A and Sanford N A 2008 *J. Cryst. Growth* **310** 3154

[37] Bertness K A, Roshko A, Mansfield L M, Harvey T A and Sanford N A 2007 *J. Cryst. Growth* **300** 94

[38] Motayed A, He M, Davydov A V, Melngailis J and Mohammad S N 2006 *J. Appl. Phys.* **100** 114310

[39] Norotsky A, Jamieson J C and Kleppa O J 1967 *Science* **158** 338

[40] Jamieson J C and Olinger B 1969 *Am. Min.* **54** 1447

[41] Zhang H Z and Banfield J F 1998 *J. Mater. Chem.* **8** 2073

[42] Zhang H Z and Banfield J F 2000 *J. Phys. Chem.* B **104** 3481

[43] Linsbigler A L, Lu G Q and Yates J T Jr 1995 *Chem. Rev.* **95** 735

[44] Tanaka K, Capule M F V and Hisanaga T 1991 *Chem. Phys. Lett.* **187** 73

[45] Zywietz T K, Neugebauer J and Scheffler M 1999 *Appl. Phys. Lett.* **74** 1695

[46] Motayed A, Bathe R, Wood M C, Ousmane S D, Vispute R D and Mohammad S N 2003 *J. Appl. Phys.* **93** 2087

[47] Lao C S, Park M-C, Kuang Q, Deng Y, Sood A K, Polla D L and Wang Z L 2007 *J. Am. Chem. Soc.* **129** 12096

[48] Sanford N A, Blanchard P T, Bertness K A, Mansfield L, Schlager J B, Sanders A W, Roshko A, Burton B B and George S M 2010 *J. Appl. Phys.* **107** 034318

[49] Garzella C, Comini E, Tempesti E, Frigeri C and Sberveglieri G 2000 *Sensors Actuators* B **68** 189

[50] Yates J T Jr 2009 *Surf. Sci.* **603** 1605

[51] Li M, Hebenstreit W, Diebold U, Henderson M A and Jennison D R 1999 *Faraday Discuss.* **114** 245

[52] Anpo M, Che M, Fubini B, Garrone E, Giamello E and Paganini M C 1999 *Top. Catal.* **8** 189

[53] de Lara-Castells M P and Krause J L 2002 *Chem. Phys. Lett.* **354** 483

[54] Henderson M A, Epling W S, Perkins C L, Peden C H F and Diebold U 1999 *J. Phys. Chem.* B **103** 5328

[55] Lee F K, Andreatta G and Benattar J-J 2007 *Appl. Phys. Lett.* **90** 181928

[56] Bikondoa O, Pang C L, Ithnin R, Muryn C A, Onishi H and Thornton G 2006 *Nat. Mater.* **5** 189

[57] Wahab H S, Bredow T and Aliwi S M 2008 *J. Mol. Chem. Struct.: Theochem.* **868** 101

[58] Perkins C L and Henderson M A 2001 *J. Phys. Chem.* B **105** 3856

[59] Thompson T L and Yates J T Jr 2006 *J. Phys. Chem.* B **110** 7431

[60] Herman G S, Dohnálek Z, Ruzycki N and Diebold U 2003 *J. Phys. Chem.* B **107** 2788

[61] Yamakata A, Ishibashi T-aki and Hiroshi O J 2002 *J. Phys. Chem.* B **106** 9122

[62] Nosaka Y, Kishimoto M and Nishino J 1998 *J. Phys. Chem.* B **102** 10279

[63] Mao Y, Schoneich C and Asmus K D 1991 *J. Phys. Chem.* **95** 80

[64] Hoffman M R, Scot T M, Wonyong C and Bahnemannt D W 1995 *Chem. Rev.* **95** 69

[65] Carp O, Huisman C L and Reller A 2004 *Prog. Solid State Chem.* **32** 33